Available online at www.sciencedirect.com
ScienceDirect
Catalysis Today 130 (2008) 411–420
CATALYSIS TODAY
www.elsevier.com/locate/cattod

Heavy crude oil hydroprocessing: A zeolite-based CoMo catalyst and its spent catalyst characterization

Mohan S. Rana *, J. Ancheyta, S.K. Maity, P. Rayo

Instituto Mexicano del Petróleo, Eje Central Lázaro Cárdenas 152, México City, D.F., 07730, Mexico

Available online 3 December 2007

Abstract

This study presents an effect of zeolite with alumina as a support for heavy oil hydroprocessing. The high surface area, moderately acidic meso- and macro-porous support was prepared with the mixing of alumina and ultra-stable Y zeolite (US-Y). The micro-structure and the composition of the zeolite crystals formed in the bulk of the alumina were examined by scanning electron microscopy with energy dispersive X-ray analysis (SEM-EDX), and there were two main crystal phases homogeneously distributed in it. A CoMo sulfide supported catalyst is evaluated for hydroconversion of Maya heavy crude oil at moderate pressure conditions. The combination of ultra-stable zeolite and alumina is able to produce bi-modal type of pores in the catalyst which may contribute to a better combination of hydrodesulfurization (HDS), hydrodemetallization (HDM) and the selective cracking of asphaltene over the acidic catalysts. The characterization of spent catalysts can help as an assistance for the selection of optimum catalyst properties along with the reactor bed length and type of catalyst pore in each bed. The strapping reaction condition indicated that the acidic catalyst for heavy oil can be used more effectively at lower temperature. An increase in temperature showed that the HDM and hydrogenation of asphaltenes (HDAs) conversions are more affected than HDS and HDN. These results indicate occurrence of a thermal cracking of complex molecules like asphaltene and metal porphyrins, which is confirmed by the gaseous selectivity of the hydrocarbons.

Keywords: HDM; HDS; HDAs; Metal sulfides; Metal deposition; Spent catalysts; Heavy crude oil; SEM-EDX; Deactivation; US-Y zeolite

1. Introduction

The demand for middle distillates fuel is increasing worldwide while its production is decreasing due to limited reserve of light petroleum. Alternatively, the productions of heavy or extra heavy crude oils are increasing in general and particularly in Mexico [1]. Thus, these low value crudes are required to be converted into more valuable products such as middle distillates. Moreover, along with other alternative fuel sources the heavy or extra heavy crude oils are considered as a major future option, which consists of different processes before refining of petroleum and commercial use of the fuels. In general, crude oils are composed of virtually infinite number of different complex hydrocarbons containing large amount of sulfur, nitrogen and metals (Ni and V). To the search of low level of these contaminants and required environmental legislation stipulation, refiners need to look for improved or new catalyst technologies, which will be able to increase the middle distillate yield as well as remove inorganic contaminants [2,3]. However, the direct processing of heavy crude oil will not produce commercial fuel, rather, it is a primary process to reduce excess metal and asphaltene content and subsequently it will be effectively used as an FCC and hydrocracking feedstock or as synthetic crude oil [4].

The main objective of this paper is to present recent results on the way for developing a catalyst for the last stage in a multi-reactor system using optimized acidic content in the catalyst. Also, other purposes are to find out what the possibilities to use such an acidic catalyst are and what the possible reaction conditions would be to effectively use a zeolite-based catalyst, particularly in the last catalyst bed where selective hydrocracking and hydrodesulfurization reactions are required, which generally demand large or even multi-modal pore size distribution [5].

It has been also recognized that due to environmental concerns and newly enacted rules and regulations, commercial products including diesel fuel must meet lower limits on contaminants to almost zero level particularly for sulfur and nitrogen. Considering these aspects of products, a wide variety

* Corresponding author. Tel.: +52 55 9175 8418; fax: +52 55 9175 8429.
E-mail address: msingh@imp.mx (M.S. Rana).

0920-5861/$ – see front matter
doi:10.1016/j.cattod.2007.10.106

of process flow schemes, operating conditions and catalysts have been used in commercial hydroprocessing, however, there is always a demand for new hydroprocessing technology which provides lower costs and improves product characteristics [6]. The refiners often produce desirable products such as middle distillates as well as lower boiling hydrocarbonaceous liquids by hydrocracking of feedstock derived from crude oil [7]. Hydrocracking is generally accomplished by acidic (due to the support) and hydrogenation functions (metallic function) under conditions of elevated pressure of hydrogen so as to yield of valuable hydrocarbon product desired by the refiner [8]. Several types of modifications are proposed to improve the acidity of catalyst particularly thereof mixed oxide [9–11] and zeolites [12,13]. The zeolite for hydrocracking is a more effective support component than mixed oxides due to its tailor making acid–base properties [11,14–17].

Ware and Wei [18] used dopants as acid–base additives of different electronic character or with different acidity to manipulate the acidity of the catalyst surface, as a result, the ratio between hydrogenation and hydrogenolysis reaction was altered. The doping elements such as sodium or cesium (alkali dopants) lowered the acidity, decreased the hydrogenolysis and metal deposition step without affecting the hydrogenation, while iodized (I) and chlorided (Cl) catalysts had high hydrogenolysis activity and low hydrogenation activity, resulting in large and strongly non-uniform nickel deposition in the catalyst, which thus reached the plugging limit more quickly than the sodium- and cesium-doped catalysts. The use of acidic catalyst was commercially demonstrated for upgrading technologies by the Cheveron/Idemitsu On-stream Catalyst Replacement (OCR)/RDS (residue HDS) units for a low price crude oil at higher feed rate and increased cracking conversion [19,20], while Ti modified US-Y zeolite was used effectively for hydrocracking of residue oil [21,22].

In this study, a method is proposed to prepare zeolite-based support extrudates with sufficient strength and balance between the textural properties and acidity of catalyst. The support was characterized via textural properties and scanning electron microscopy (SEM) for morphology and composition. The characterizations of spent catalyst were carried out by N_2 adsorption–desorption, and SEM-EDX. The results point out that the deactivation takes place mainly on the surface of catalyst due to coke and metal depositions although with increasing temperature up to 420 °C, reactor plugging occurred most likely due to coke formation or asphaltene precipitation by the presence of large amounts of low molecular weight (C_1–C_4) hydrocarbons formed during reaction. The spent catalyst characterization (carbon and metal deposition along the reactor length) gives a better understanding of the heavy oil hydroprocessing reactions and the role of deposited species in order to further understand or design catalysts and reactors loading to achieve longer stability of the catalyst with time-on-stream.

2. Experimental

The dry extrudates of commercial alumina boehmite (Catapal C1 and Catapal 200) and US-Y zeolite support were prepared using 5% (v/v) HNO_3 in H_2O for peptization of alumina. The extrudates were subsequently dried and calcined at 550 °C for 4 h. The detailed composition and synthesis of support extrudate are shown in Table 1 and Fig. 1, respectively.

Table 1
Properties and composition of CoMo/Al_2O_3+US-Y zeolite-based catalyst

Support composition (wt.%)	
US-Y zeolite	25
Al_2O_3 in support (Catapal 200)	25
Al_2O_3 in support (Catapal C1)	50
Na_2O	0.02
Catalyst composition (wt.%)	
Mo	7.4
Co	2.0
[Co/(Co + Mo)]	0.3
Catalyst physical properties	
Shape	Cylindrical extrudate
Size (in.)	1/12
Specific surface area (m^2/g)	182.7
Average pore diameter (nm)	6.8
Total pore volume (mL/g)	0.31

The molybdenum-supported catalysts were prepared by the incipient wetness impregnation method. An appropriate amount of ammonium heptamolybdate was used and dissolved in ammonia solution. The Co promoted catalyst was also prepared via the sequential impregnation procedure on Mo-loaded catalysts (dried at 120 °C and calcined at 400 °C). The cobalt nitrate salts were impregnated in an aqueous medium. The final catalysts were dried in presence of air at 120 °C

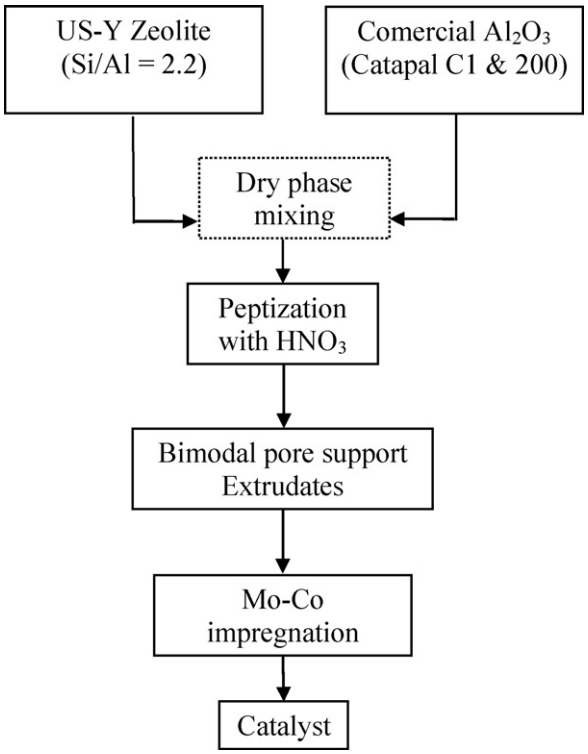

Fig. 1. Flowchart of the synthesis of Al_2O_3-US-Y zeolite (75–25, wt.%) catalyst.

overnight and calcined at 450 °C for 4 h. The composition of supported catalysts is reported in Table 1.

The BET specific surface area (SSA), pore volume (PV), and pore size distribution (PSD) analyses were carried out in Quantochrome Nova 4000 equipment. Nitrogen gas was employed for SSA measurements at liquid nitrogen temperature (−196 °C). Prior to the adsorption, the samples were degassed for 3 h at 300 °C.

The catalyst pretreatment and the hydrotreating reactions were both carried out in high pressure integral fixed-bed up-flow reactor. The reactor was loaded with 10 mL oxidic catalyst with 3–5 mm extrudate size diluted with an equal volume of SiC. The catalyst was sulfided *in situ* using a mixture of dimethyldisulfide (DMDS), straight run gas oil (SRGO), and H_2. After hermiticity test and depressurizing the reactor to atmospheric pressure, the sulfiding feed (S ≈ 2 wt.%) was started at room temperature and atmospheric pressure in order to wet the catalyst. The liquid was drained after 4 h, and then the temperature rose linearly from 30 °C to 120 °C (30 °C/h) and remained for 2 h. Later, the temperature was increased at the rate of 30 °C/h until it reached 150 °C, at 2.8 MPa pressure and remained as such for 2 h. The temperature was further increased to 260 °C and remained as such for 3 h. The final temperature of sulfidation was 320 °C, which was stabilized for 5 h at 2.8 MPa. After sulfidation, the flow was switched to the Maya crude feedstock (Table 2) and the operating conditions were adjusted as reported in Table 3. These moderate severity conditions were selected based on the literature as well as on our own experience working with heavy and extra heavy crude [1,6].

Metals (Ni, V) were analyzed in the feed and products using flame atomic adsorption spectrometry (ASTM D 5863-00a method). The total S content was determined with a HORIBA model SLFA-2100/2800, using scattered spectroscopy by sulfur, generating energy dispersive X-ray fluorescence. The X-ray beam was separated selectively with the help of a filter and detected as sulfur concentration. Nitrogen was measured by oxidative combustion and chemiluminescence (ASTM D 4629-02 method) at high temperature combustion in an oxygen rich atmosphere. Asphaltene is defined as the insoluble fraction in *n*-heptane, which is an indirect measure of dry-sludge formation. The conversion of HDS, HDM, HDN and HDAs was determined as:

$$\%\,\text{Conversion} = \frac{C_{\text{Feed}} - C_{\text{Product}}}{C_{\text{Feed}}} \times 100$$

where C_{Feed} is the initial concentration of sulfur, metal, nitrogen or asphaltene in the feedstock while C_{Product} is the final concentration in the product.

The surface deposits of catalysts were studied by means of elemental analysis with the SEM-EDX analytical instrument xT Nova NanoLab 200 (FEI Schottky FEG, 30-1 keV), combined with a dual high resolution focused ion beam (Ga + FIB) using detector type SUTW, Sapphire with LEAP+ crystals for the best light element performance of the Si(Li) detector. The sample was deposited on a carbon holder and evacuated at high vacuum (10^{-5} Torr) before images were taken. Five representative analyses were taken to confirm the results. The analysis was made across the radial line of the extrudate and elemental mapping of electron back-scattering (EBS) microphotography and point-by-point microanalysis of the dispersion energies were reported.

Table 2
Typical properties of Maya heavy crude oil

Properties	Feedstock
Elemental analysis	
C (wt.%)	86.9
H (wt.%)	5.3
N (wt.%)	0.3
S (wt.%)	3.52
Metal (wppm)	
Ni	49.5
V	273.0
(Ni + V)	322.5
Ca	11.26
Mg	2.04
Na	44.83
K	20.25
Fe	2.16
Asphaltene, wt.% (*n*-C_7 insol.)	12.7
Physical properties	
Specific gravity 20/4 °C	0.9251
Ramscarbon (wt.%)	10.87
API gravity	21.31

Table 3
Reaction conditions for fixed-bed integral reactors

Conditions	
Temperature (°C)	380–420
Pressure (MPa)	7.0
Hydrogen flow (l/h)	4.6
Flow of Maya crude (mL/h)	10
LHSV (h^{-1})	1.0
Hydrogen/Oil ratio (m^3/m^3)	56.63
Mode of operation	Up-flow
Time-on-stream (h)	204
Catalyst volume, mL (g)	10 (6.8)
Extrudate diameter (mm)	2.2
Extrudate length (mm)	5–7
Crushing strength (kg)	2.8
Feed composition tested	Pure Maya crude

3. Results and discussion

3.1. Synthesis of support and characterization of fresh catalyst

An optimum concentration of US-Y zeolite (25 wt.%) in support was studied and the solid prepared by dry extrusion using a mixture of crystalline zeolite and inorganic binder alumina (filler), which provide favorable mechanical strength to the extrudate during molding and after preparation. The distribution of acid site in binders decreases the efficiency of the acid sites by hindering the accessibility to the zeolite on the surface in the form of bulk. Thus, a great effort has been

devoted to obtain mechanical properties of the extrudate mainly with respect to the heavy oil hydroprocessing. Thus, the use of alumina is to improve properties like textural, molding or mechanical strength of support and distribute zeolite acid sites homogeneously at the interior part of the catalyst to avoid fast deactivation of the catalyst [23]. The zeolites at the outer surface of the catalyst may enhance deactivation due to the cracking activity (i.e., acidity) of complex hydrocarbons such as asphaltene (12 wt.% in Maya crude) molecules that are very large and have multiple stacked layers, containing large numbers of contaminants (high metals, S, N and conradson carbon residue contents), which easily deactivate the catalysts [24]. Hence, catalyst deactivation by coke and metal deposition in heavy oil catalytic hydroprocessing remains a serious problem [24,25].

There are few reports which demonstrate a methodology for the preparation of zeolite structures in a desired geometry without using binders of high purity with moderate mechanical strength and bimodal pore size distribution [26]. However, some of them include rather delicate steps such as the preformed gel particles produced by treating silica sol with an organic liquid to obtain a dense gel, which is then shaped into tiny beads by subsequent dropping it into oil [27,28]. Additionally, using zeolite high specific surface area (SSA) a balance between the textural properties such as micro-, meso- and macro-porous is obtained. The support was prepared in this work using the mixing of different alumina (meso- and macro-pores) with US-Y zeolite that has most of the pores in the range of meso (88%) and macro (9%) as shown in Table 4. The moderate acidity character of the catalyst introduced by the zeolite has positive effect on the hydrodemetallization as well as asphaltenes conversion [29,30]. It was considered that an optimum amount of zeolite in the catalyst, particularly at the interior part of catalyst, can improve the cracking function without rapid deactivation. The microstructure and the composition of the silica crystals were formed in bulk of the alumina, which were identified by SEM-EDX, and there were two main crystal phases homogeneously distributed in it. The composition of support was examined by SEM-EDX that confirmed the presence of small particles of zeolite using elemental mapping of catalyst matrix as shown in Fig. 2. These results indicated that the zeolite is distributed proportionally as a lumped shape or micro-structures into the alumina matrix. Moreover, the silica distribution is carried out for different level of catalyst loaded at the top and bottom of the reactor. The silica SEM-EDX analysis of catalyst indicates that composition of the Al and Si can be further improved by the careful mixing of zeolite (Si) into the bulk of alumina to ensure the better representative of silica distribution.

In Fig. 3, from N_2 adsorption–desorption isotherms, it is evident that CoMo catalyst contains meso- and macro-pores. The pore size distribution (PSD) of the fresh catalyst is also shown in the same figure. The isotherm is of type IV [31,32] and the pore size distribution in the range of micro-pores (<2 nm) was very low, while relatively more pores are in the range of meso- as well as macro-pore regions. The adsorption–desorption isotherms and the corresponding pore size distributions for spent catalyst followed a different pattern, which will be explained in later section. The average pore diameter (APD) of fresh catalyst, determined according to the BJH model [31] was 6.8 nm. Moreover, the catalyst showed bi-modal type of pores, which is particularly designed for the heavy oil hydroprocessing to obtain a balanced activity for hydrodemetallization and hydrodesulfurization. The bi-modal pore is a combination of meso- and macro-pores in the range of 5 nm and 12 nm, respectively. The preparation steps such as optimum composition, mixing of different support components, and concentration of peptizing agent (HNO_3) were developed with respect to an industrial point of view to obtain advantageous acidity and textural properties of porous solids basically having bi-modal pore size distribution; each step of support preparation influences in different way to construct textural properties of the carrier which results in meso- and macro-pores diameter.

3.2. Catalytic activity

Fig. 4 shows the results of catalytic activity of the CoMo catalyst at micro-flow evaluation scale using Maya crude heavy oil. HDS, HDN, HDM and HDAs conversions are presented as

Table 4
Textural properties of spent catalyst

Properties	Fresh	Spent catalysts (% loading catalyst bed)				
		Cat-1 (0)	Cat-2 (25)	Cat-3 (50)	Cat-4 (75)	Cat-5 (100)
SSA (m^2/g)	182.7	91.1	49.7	40.5	49.2	43.3
TPV (mL/g)	0.31	0.25	0.08	0.07	0.08	0.08
APD[a] (nm)	6.2 (bi-modal)	11.3	6.9	5.6	6.6	5.6
Pore size (nm) distribution (%)						
<2	1.7	5.9	5.7	15.9	18.2	18.1
2–5	15.7	14.6	17.2	18.7	18.6	23.9
5–10	35.8	30.2	38.7	38.4	37.5	34.2
10–25	37.4	41.4	28.1	21.1	21.1	17.9
25–50	6.1	3.9	5.2	2.5	1.9	2.7
50–100	2.9	2.1	4.0	1.6	1.6	1.8
>100	0.4	1.8	1.0	1.7	1.1	1.2

[a] Average pore diameter (pores based on 4V/S). Cat-1, 2, 3, 4 and 5 indicated the catalyst bed length.

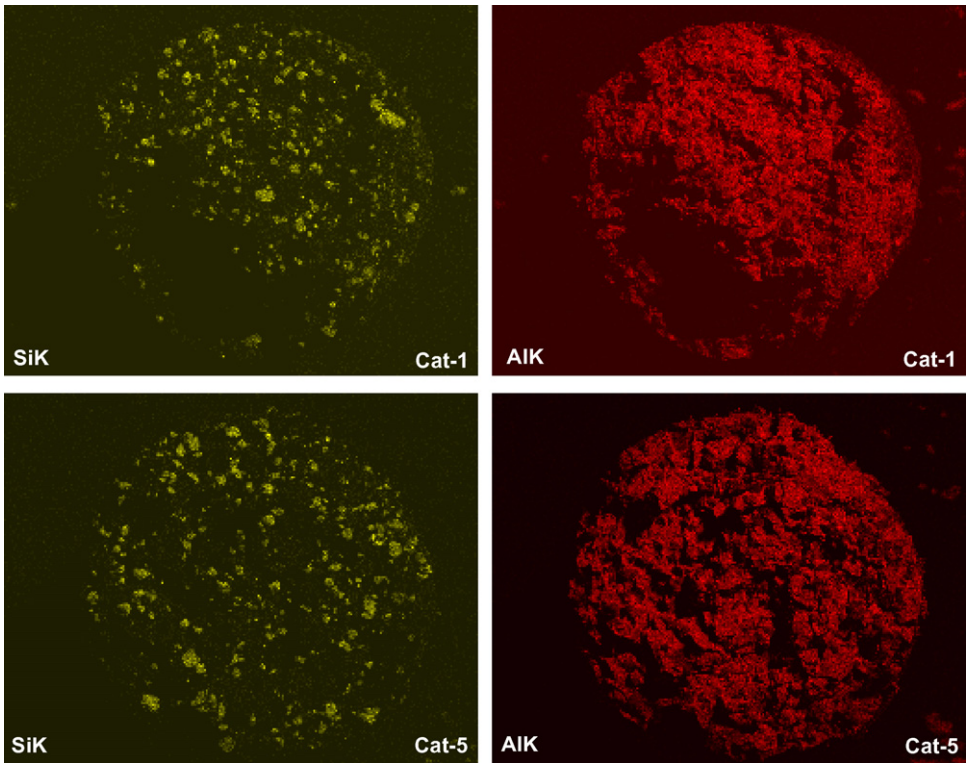

Fig. 2. Scanning electron X-ray micro-analyzer indication of silica and alumina distribution (zeolite) into the alumina matrix using dry extrusion for support preparation.

a function of time-on-stream at different temperatures. The catalytic results indicate that the catalyst is more active for hydrogenolysis (HDM, HDS, HDN) than hydrogenation (HDAs) function, which could be due to the CoMo active metal. In general strong hydrogenation function in the first reactor is not used for this study because the hydrogenation may increase paraffin hydrocarbons, which favor the asphaltenes precipitation. On the other hand, direct hydrogenation of asphaltenes is very significant to slacken the complex molecule and exposed metals (Ni and V) and nitrogen to the catalytic sites. The catalyst stability against TOS at 380 °C followed the same kind of deactivation tendencies for HDS, HDN, HDM and HDAs [1,33,34]. After the activities stabilize at 380 °C, the temperature of reactor was increased to 400 °C. The activities with TOS remained almost constant for 80 h, thus, the stability of catalyst at this temperature (i.e., 400 °C) was relatively good, which may be due to the initial deactivation by coke deposition (i.e., acidity) stage that was conceded at 380 °C. The temperature was then further increased (420 °C) in order to find out the possible role of temperature. Unfortunately at this

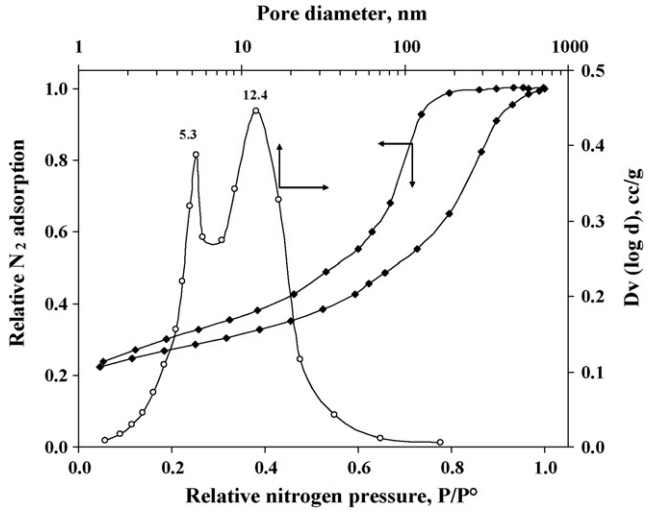

Fig. 3. Fresh catalyst adsorption–desorption isotherms and bi-modal pore size distribution for CoMo/γ-Al_2O_3-US-Y catalyst.

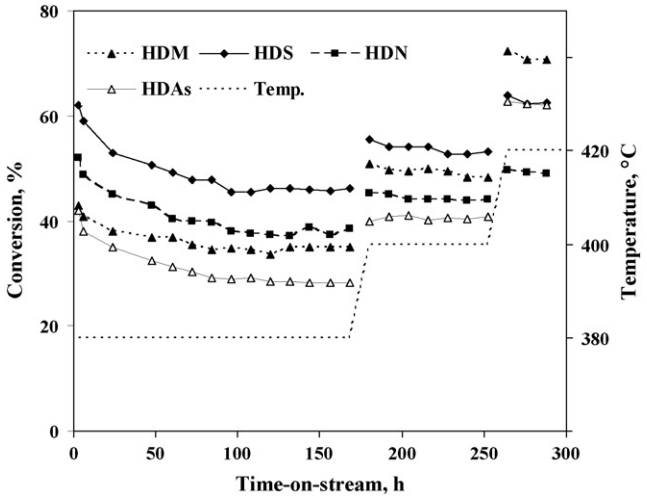

Fig. 4. Catalytic activities of supported CoMo/γ-Al_2O_3-US-Y zeolite with time-on-stream at different temperatures.

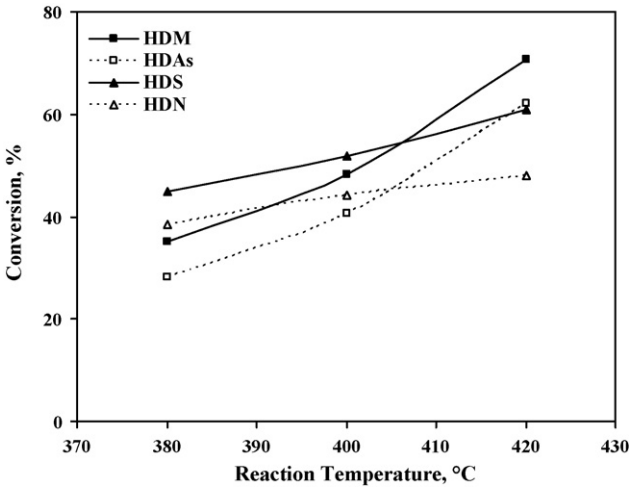

Fig. 5. Effect of temperature on catalytic activities.

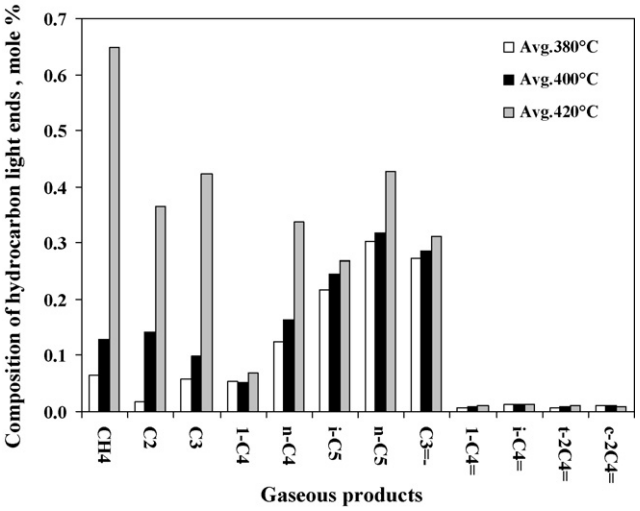

Fig. 6. Composition of light gases in the product.

temperature only few balances were collected because of high pressure drops ($\Delta P \approx 5$ MPa) and as a consequence permanent shut-down was required. The promising justification for such a high ΔP is due to the excess of cracking; whose gaseous hydrocarbon paraffins (C_1–C_3) may precipitate asphaltenes or form sediments at high temperature. Thus, at 420 °C, the pressure drop reached such a limit that the catalyst necessarily required unloading. A comparison between the steady state activities at different temperatures is shown in Fig. 5. The behavior with increasing temperature indicated that HDS and HDN activities followed different reaction mechanism compared with HDM and HDAs. At temperature higher than 400 °C reaction is dominated by thermal cracking (hydrocracking) while at temperature lower than 400 °C reaction is subjected to the hydrogenation route.

At lower temperature (380 °C) the catalyst is selectively good for HDS activity (1.3 times higher than HDM) most likely due to the role of catalytic sites. With increasing the temperature to 400 °C, the HDS selectivity remains 1.09 times higher than HDM while at 420 °C the HDM reaction becomes more selective than HDS. As an effect of temperature HDAs reaction followed the same tendency as HDM reaction, which indicates that HDM and HDAs activities are controlled by the temperature while HDN and HDS reactions are based on the number of catalytic sites. HDM and HDAs conversions follow similar behavior since most of the metals are associated with asphaltenes, which are located at the internal part of the molecules and thus conversion of asphaltenes has to proceed before HDM conversion. The cracking activity results of different temperatures are confirmed by the light gaseous product formation as shown in Fig. 6. The relative increase in light gaseous product selectivity with temperature (380–420 °C) is shown in Fig. 7, the cracking activities most probably occur on the paraffinic alkyl side chains of asphaltenes [1,35]. The relative gaseous yield was defined as gaseous product composition at 420 °C (400 °C) divided by the corresponding composition at 380 °C. The gaseous paraffinic products also have adverse effect on the unconverted asphaltene, which precipitates at the end or exit line of the reactor, because

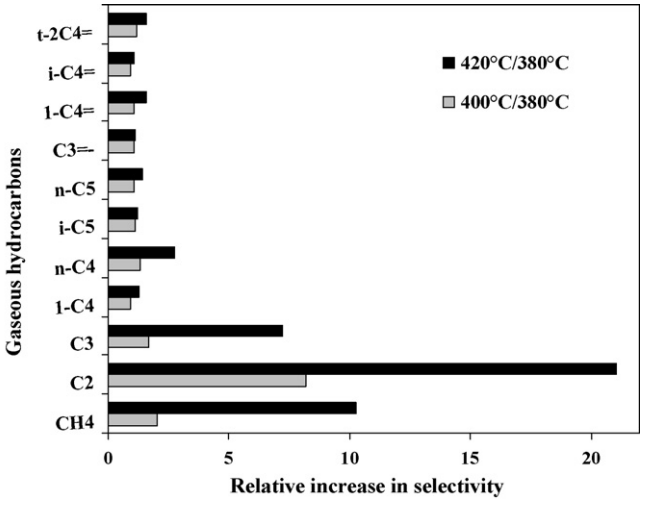

Fig. 7. Relative increase in selectivity with respect to temperature.

paraffins may cause asphaltene precipitation at room temperature [36], which further enhances the pressure drop and line plugging. Thus, in this study the high temperature toward end of run leads to coke (sediment) formation and deactivation of catalyst, the former is a solid material which is able to plug the inlet-outlet of the reactor. The sludge (sediment) formation usually occurs at high temperature and is due to changes in relative solubility of asphaltenes, maltenes and other paraffinic products. Andersen [37] reported that sludge formation is owed to the critical solubility parameter of the solvent–precipitant mixture at which the least soluble asphaltene will precipitate or separate. Recently, Bartholdy and Andersen [38] studied that sludge formation occurs at high temperature and concluded that it is mainly due to the chemistry of maltenes and asphaltenes. They have reported that as the temperature increased, the critical solubility parameter also increased indicating an augmentation in the asphaltene solubility parameter, which agrees with the reduction in H/C ratio that are representative of a thicker structure like *catacondensed polycyclic* and/or *pericondensed polycyclic aromatic* hydrocarbons.

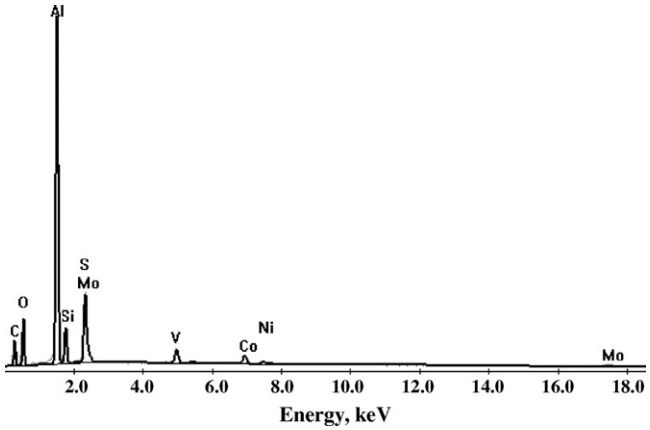

Fig. 8. Global composition of top bed spent catalyst.

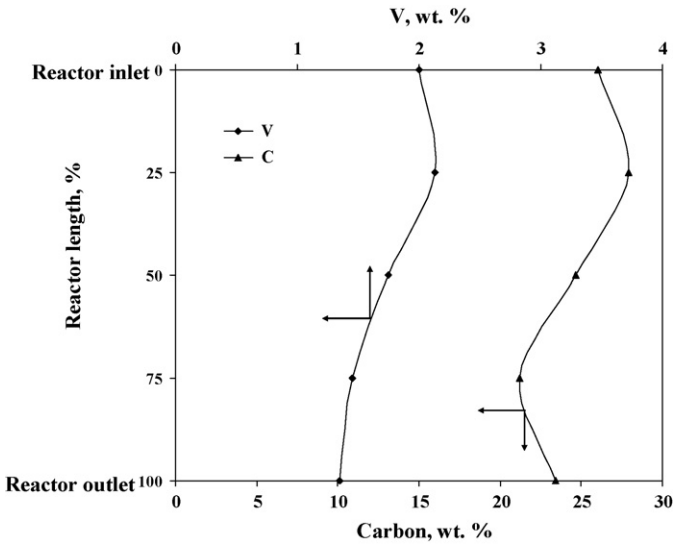

Fig. 9. SEM-EDX analysis of spent catalyst carbon and vanadium distribution along with catalyst bed-depth.

3.3. Spent catalyst characterization

To determine the composition and homogeneity of spent catalysts they were characterized by scanning electron microscopy with energy-dispersed analysis of X-ray, using

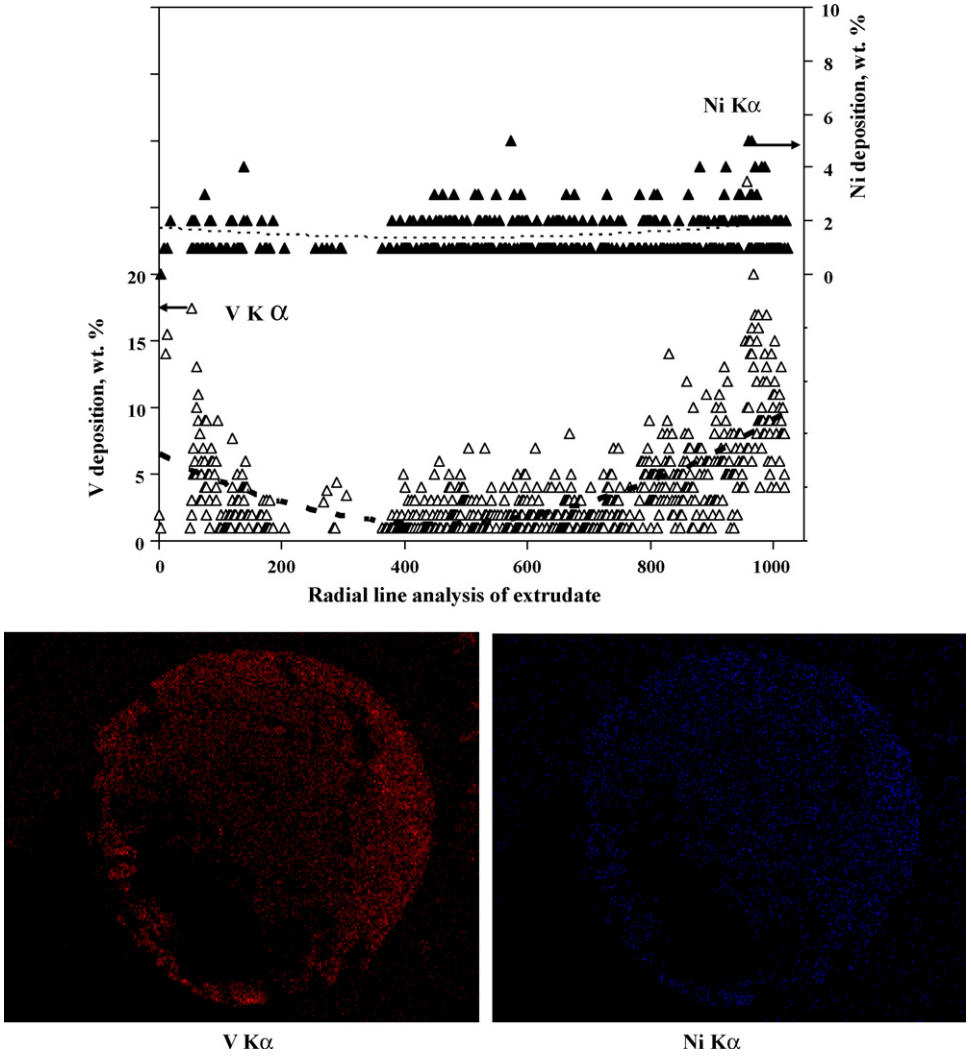

Fig. 10. Radial distribution of Vanadium (VKα) and Nickel (NiKα) along the extrudate.

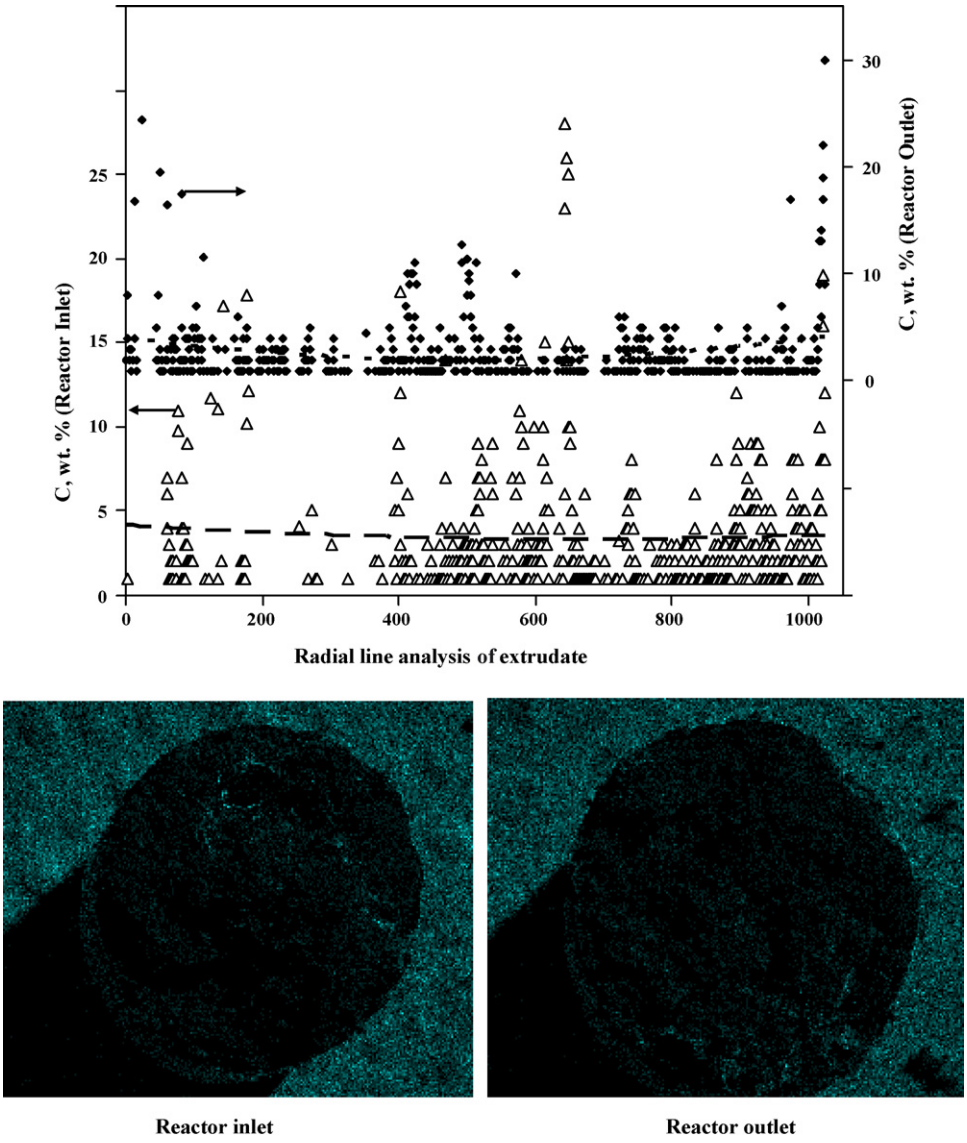

Fig. 11. Spent catalyst SEM-EDX: radial distribution of carbon along the extrudate.

electron probe microanalysis methods that estimated the crystal size, morphology, and elemental composition of the catalyst [39–42,18]. Compared with other techniques, the EDX analysis succumbs accurate information on surface as well as quantitative results featuring all the elements present in the support, fresh catalyst and spent catalyst, specifically, C, O, Al, S, V, Ni, Mo, Co, etc., by their $K\alpha$ (in the case of Mo $K\alpha$ and L) X-ray emission lines (keV) as shown in Fig. 8. Particularly, the surface deposition (V and C) during the reaction along with the reactor length is shown in Fig. 9. The figure shows that the spent catalyst V and carbon are highly concentrated on the surface of the catalyst, whose concentration increased in the first part of the reactor and exhibited maximum values at around 25% of the total reactor bed-depth. It is expected that the deposition of carbon and metal at around 25% bed-depth is due to the asphaltenes cracking, which is more controlled by the temperature than the catalytic reaction [43]. Similar kinds of results were reported by Fleisch et al. [44] for V deposition, while carbon deposition was increasing with weight percent of catalyst loading. Recently, Takashi et al. [45] reported that carbon is distributed evenly along the reactor length. The deposition of metal, particularly vanadium, is observed throughout the reactor bed length, while Ni was deposited in traceable concentration only at the top-bed of the catalyst. The distribution profile of sulfided particles of Ni and V is confirmed by EDX on the surface of catalyst. At the top of reactor nickel sulfide species were relatively uniformly dispersed while larger particles or higher concentrations of V deposition are present on the surface of extrudate, with smaller amounts at the interior as shown in Fig. 10. Moreover, the carbon film has very low backscattered electron acquiesce compared with that from the particle, thus the backscattered electron mode of the particle image is seen with very high contrast, which demonstrated the individual mapping of particles particularly for deposited metals such as nickel and vanadium. However, carbon deposition resulted relatively uniformly distributed through the reactor bed length as shown in Fig. 11.

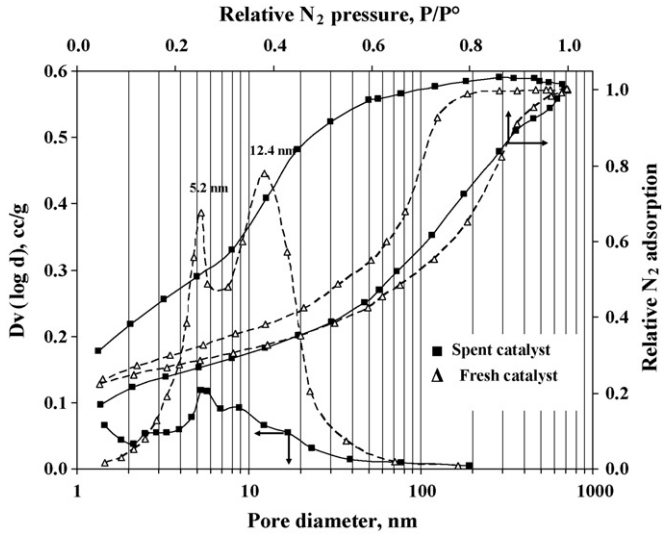

Fig. 12. Fresh and spent catalysts adsorption–desorption isotherms and pore size distribution.

The spent catalyst deactivation (i.e., depositions of carbon and metals) is also confirmed by the textural properties, which show 70–80% decrease as presented in Table 4. The decrease in textural properties indicates that deposited species significantly altered the pore structure. Obviously, the way in which the metals are deposited (SEM-EDX results) and the percentage of decrease in textural properties clearly indicated that the deactivation seriously poisons external surface of the catalyst and most of the pore are close at the pore mouth. However, these analyses do not reveal how the pores are changing. To confirm these results, the adsorption–desorption isotherm of spent catalyst is drawn and compared with that of fresh catalyst in Fig. 12. The comparison of isotherms indicates that the deposited species are either totally close the pore or partially close the pore of the catalyst. A large increase in the hysteresis loop also confirms the deactivation at pore mouth, which could prevent the maximum utilization of internal surface of the catalyst, and consequently, blocks the active sites. The most common deactivation is either due to the blocking of catalytic sites by deposition of species or due to the reactant diffusion limitation, which is more severe than the previous one. Fig. 12 also represents a decrease in pore diameter, which occurs in the range of 5–12 nm.

4. Conclusion

A method was proposed to prepare high surface area, reasonable mechanical strength, moderate acidity, meso- and bi-modal pore diameter support by the physical mixing of alumina and US-Y zeolite. The bi-modal type of pore in the catalyst contributed to the combination of hydrodesulfurization (HDS), hydrodemetallization (HDM) and the selective hydroracking of asphaltenes over the acidic catalyst. The severe reaction setting indicated that the acidic catalyst can only be effectively used at lower temperature or moderate operating conditions. An increase in temperature specifies that HDM and HDAs reaction rates are faster than HDS and HDN ones, thus, the results sustain a thermal cracking of complex molecules like asphaltene and metal porphyrins, which is also confirmed by the gaseous product selectivity of the hydrocarbon. The high gaseous product yield for heavy oil processing enhances asphaltene deposition and sediment formation. The deactivation of catalyst occurs due to the metal and carbon deposition over the catalyst. The distribution of carbon was relatively uniform through the reactor bed while the metals are deposited maximum at around 25% of reactor bed length. The vanadium metal sulfide is preferentially deposited on the external surface of the catalyst while nickel sulfide is distributed homogeneously in the extrudate.

References

[1] M.S. Rana, S.K. Maity, J. Ancheyta, Maya heavy crude oil hydroprocessing catalysts, in: J. Ancheyta, J.G. Speight (Eds.), Hydroprocessing Heavy Oil and Residua, Taylor & Francis, New York, 2007, Chapter 7.
[2] A. Espinosa, P.H. Bigeard, P. Marion, Oil Gas Sci. Technol. Revue de l'IFP 49 (1994) 529–539.
[3] J. Scherzer, Octane-Enhancing Zeolite FCC Catalysts, Scientific and Technical Aspects, Marcel Dekker, New York, 1990.
[4] J. Ancheyta, M.S. Rana, E. Furimsky, Catal. Today 109 (2005) 1–2.
[5] H. Toulhoat, D. Hudebine, P. Raybaud, D. Guillaume, S. Kressmann, Catal. Today 109 (2005) 135–153.
[6] J. Ramírez, M.S. Rana, J. Ancheyta, Characteristics of heavy oil hydroprocessing catalysts, in: J. Ancheyta, J.G. Speight (Eds.), Hydroprocessing Heavy Oil and Residua, Taylor & Francis, New York, 2007, Chapter 6.
[7] J. Scherzer, A.J. Gruia, Hydrocracking Science and Technology, Marcel Dekker, New York, 1996.
[8] J. Ward, Hydrocracking processes and catalysts, Fuel Process. Technol. 35 (1993) 55–85.
[9] R.C. Hansford, Silica-zirconia-titania hydrocracking catalyst, US Patent 3,159,588 (1964).
[10] J. Jaffe, Coprecipitation method for making multi-component catalysts, US Patent 3,401,125 (1968).
[11] A. Nishijima, H. Shimada, T. Sato, Y. Yoshimura, J. Hiraishi, Polyhedron 5 (1986) 243–247.
[12] I.E. Maxwell, Catal. Today 1 (1987) 385–413.
[13] R.S. Mann, I.S. Sambi, K.C. Khulbe, Ind. Eng. Chem. Res. 27 (1988) 1788–1792.
[14] B. Egia, J.F. Cambra, P.L. Arias, M.B. Güemez, J.A. Legarreta, B. Pawelec, J.L.G. Fierro, Appl. Catal. A. Gen. 169 (1998) 37–53.
[15] A. Corma, J. Catal. 216 (2003) 298–312.
[16] A. Corma, Chem. Rev. 97 (1997) 2373–2420.
[17] C. Leyva, M.S. Rana, F. Trejo, J. Ancheyta, Ind. Eng. Chem. Res. 46 (2007) 7448–7466.
[18] R.A. Ware, J. Wei, J. Catal. 93 (1985) 135–151.
[19] R.W. Bachtel, K. Shinmura, B.E. Reynolds, R. Pardoe, D.E. Earls, J. Chabot, Chevron OCR (Onstream Catalyst Replacement) process, AIChE 1995 Spring National Meeting (Houston 3/19-23/95) Preprint N.46f 17P.
[20] B.E. Reynolds, K. Yagi, R.W. Bachtel, Chevron onstream catalyst replacement (OCR) provides enhanced flexibility to residue hydrotreaters, NPRA 1992 Annual Meeting (New Orleans 3/22-24/92) AM-92-61 22P.
[21] N. Ohshio, T. Enomoto, K. Honna, H. Ueki, Y. Hashimoto, H. Aizono, M. Yoshimoto, H. Shimada, Fuel 83 (2004) 1895–1898.
[22] T. Enomoto, H. Aizono, H. Ueki, Y. Hashimo, N. Oshio, K. Honna, M. Yoshimoto, H. Shimada, J. Jpn. Pet. Inst. 47 (2004) 239–248.
[23] I. Mochida, I.J-Koo, Y.S-Ho, Comprehensive approaches to heavy oil upgrading, in: J. Ancheyta, G.F. Forment (Eds.), Proceedings of the International Symposium on Advances in Hydroprocessing of Heavy Oil Fractions (ISAHOF-2007), Morelia, Mexico, 26–29 June, 2007.
[24] C.H. Bartholomew, Catalyst deactivation in hydrotreating of residua: a review, in: M.C. Oballa, S.S. Shih (Eds.), Catalytic Hydroprocessing of Petroleum and Distillates, Marcel Dekker, Inc., New York, 1994.

[25] J.W. Gosselink, CatTech 2 (2) (1998) 127–144.
[26] A. Ozcan, H. Kalıpcüılar, Ind. Eng. Chem. Res. 45 (2006) 4977–4984.
[27] E. Michalko, Method for Preparing Spherically Shaped Crystalline Zeolite Particles. U.S. Patent No. 3,386,802 (1968).
[28] E. Michalko, Method for Producing Molecular Sieve Zeolite Particles. U.S. Patent No. 3,356,451 (1967).
[29] P. Rayo, J. Ramírez, J. Ancheyta, M.S. Rana, Petr. Sci. Technol. 25 (1/2) (2007) 215–230.
[30] K. Honna, Y. Araki, T. Enomoto, M. Yoshimoto, Y. Nishimura, H. Shimada, J. Japan Petr. Inst. 48 (4) (2005) 189–196.
[31] C.T. Kresge, M.E. Leonowicz, W.J. Roth, J.C. Vartuli, J.S. Beck, Nature 359 (1992) 710.
[32] S.J. Gregg, K.S.W. Sing, Adsorption, Surface Area and Porosity, Academic Press, London, 1982.
[33] M.S. Rana, J. Ancheyta, P. Rayo, Catal. Today 109 (2005) 24–32.
[34] D.S. Thakur, M.G. Thomas, Appl. Catal. 15 (1985) 197–225.
[35] J. Ancheyta, M.S. Rana, E. Furimsky, Catal. Today 109 (2005) 3–15.
[36] D.L. Mitchell, J.G. Speight, Fuel 52 (1973) 149–152.
[37] S.I. Andersen, Energy Fuels 13 (1999) 315–322.
[38] J. Bartholdy, S.I. Andersen, Energy Fuels 14 (2000) 52–55.
[39] M.S. Rana, J. Ancheyta, P. Rayo, Catal. Today 104 (2005) 86–93.
[40] R.T. Galiasso, L. Caprioli, Catal. Today 109 (2005) 185–194.
[41] H. Toulhoat, R. Szymanski, J.C. Plumail, Catal. Today 7 (1990) 531–568.
[42] C.-W. Hung, J. Wei, Ind. Eng. Chem. Process Dev. 19 (1980) 250–263.
[43] R. Tanaka, J.E. Hunt, R.E. Winans, P. Thiyagarajan, S. Sato, T. Takanohashi, Energy Fuels 17 (2003) 127–134.
[44] T.H. Fleisch, B.L. Meyers, J.B. Hall, G.L. Ott, J. Catal. 86 (1984) 147–157.
[45] T. Takashi, H. Higashi, T. Kai, Catal. Today 104 (2005) 76–85.